An Estimation Method for the Overthrowing Moment of Vehicles on the Car Deck of the Ro-Ro Ferry

Alamsyah
Department of Naval Architecture, Kalimantan Institute of Technology, Balikpapan, Indonesia | Center of Maritime Infrastructure Engineering, Kalimantan Institute of Technology, Balikpapan, Indonesia
alamsyah@lecturer.itk.ac.id (corresponding author)

Suardi
Department of Naval Architecture, Kalimantan Institute of Technology, Balikpapan, Indonesia
suardi@lecturer.itk.ac.id

Wira Setiawan
Department of Naval Architecture, Kalimantan Institute of Technology, Balikpapan, Indonesia
wira@lecturer.itk.ac.id

M. Uswah Pawara
Department of Naval Architecture, Kalimantan Institute of Technology, Balikpapan, Indonesia
uswah.pawara@lecturer.itk.ac.id

Hariyono
Department of Naval Architecture, Kalimantan Institute of Technology, Balikpapan, Indonesia
hariyono@lecturer.itk.ac.id

Nurbaya
Department of Naval Architecture, Kalimantan Institute of Technology, Balikpapan, Indonesia
09201036@student.itk.ac.id

Daeng Paroka
Department of Ocean Engineering, Engineering Faculty, Hasanuddin University, Gowa Regency, Indonesia
dparoka@eng.unhas.ac.id

Andi Ardianti
Department of Naval Architecture, Engineering Faculty, Hasanuddin University, Gowa Regency, Indonesia
a.ardianti@unhas.ac.id

Received: 1 September 2024 | Revised: 16 November 2024 | Accepted: 23 November 2024

 DOI: https://doi.org/10.48084/etasr.8887

ABSTRACT

Ensuring passenger safety and comfort is crucial for maintaining trust in sea transportation, especially as ship accidents remain a concern. One critical area for improvement is the vehicle fastening systems on Roll-On-/Roll-Off (Ro-Ro) ferries, which must account for fastening techniques and vehicle positioning to prevent shifting or overturning during adverse conditions. This study calculates the shear and overturning moments acting on vehicles when a ferry experiences rolling motion due to beam waves, using numerical

simulations to evaluate the impact of vehicle placement. Wave heights were adjusted to reflect operational area conditions, and vertical and lateral accelerations were derived based on vehicle dimensions, type, and enter of gravity. A case study of a Ro-Ro ferry operating on the Bira-Pamatata route revealed that Bus 2, located at the rear centreline, exhibited the highest rolling moment of 14,370 N·m, while Ayla 21, positioned at the front centreline, had the lowest moment of 1,141 N m. These results demonstrate that vehicle mass, dimension, and vertical and horizontal center of gravity significantly influence rolling and share moments.

Keywords-ship roll; ro-ro ferry; car deck; moment rolling; acceleration

I. INTRODUCTION

Indonesia, the world's largest archipelago, is a nation where two-thirds of the country is covered by the sea. With the increasing need of people using marine transportation, ship accidents remain a pressing concern, claiming countless lives each year [1]. One of the main factors causing these accidents is the ship rolling in random waves, which is a complicated nonlinear motion that contributes substantially to ship instability and capsizing. Previous research has provided valuable insights into the dynamics of ship rollovers with various approaches having been employed to better understand and predict these events. Authors in [2], approached the problem using the Finite Element Method (FEM), solving the Fokker-Planck (FP) equations numerically for homoclinic and heteroclinic ship rollover under random waves, which are described as repeated white noise and Gaussian wave excitations. In [3], ship rollover events were predicted through the employment of a data-driven ship motion forecast method, while in [4], a ship rollover behavior was observed by simulating the load distribution located on the centerline side and even further away from it, deploying an experimental method in a test tank. Simultaneously, authors in [5] utilized a hybrid data-driven method by applying a combination of low-fidelity physics with Machine Learning (ML) to model nonlinear forces and moments at a reduced computation cost. In [6], a simple model for ship stability based on Mathieu equation was employed, namely a second-order differential equation with periodic coefficients, which describes the phenomenon of parametric rolling. In addition to the studies on ship rollovers, several other investigations have focused on the effects of ship rolling motion and its impact on stability, passenger movement, and safety. Specifically, authors in [7] identified the effect of ship rolling motion on the speed of passengers on board, finding that the farther passengers are from the ship's center of gravity, the lower is their speed during rolling. Similarly, in [8], the human evacuation speed during a ship rolling event was predicted, with a focus placed on the accommodation deck and dining areas of passenger ships. In [9], the stability behavior and rolling periods of ferry RO-RO ships were studied by varying the types of electric and conventional vehicles, considering different weight distributions. A potential consequence of a Ro-Ro ferry's rolling motion is the possibility for the items on the vehicle deck to shift. When a car moves or rolls to one side of the deck, it can cause an initial tilt, which in turn affects the ship's stability and can lead to capsizing [10]. This risk is more likely to happen under poor sailing conditions. The geometry and center of gravity of an object relative to the baseline determine its transverse displacement [11, 12]. To address these risks, the government has implemented regulations regarding shipboard vehicle attachment systems [13, 14]. Although these standards specify how different types of vehicles must be secured during sailing, their application has not been proven effective on short routes. Consequently, research into the potential for vehicle shifting on Ro-Ro ferries, as well as the arrangement of the vehicle fastening design system and its effect on ship safety during sailing, are vital [15-19]. The likelihood of vehicles moving or overturning on Ro-Ro ferries depends on the lateral acceleration due to ship motion as a function of their position on the ship [20]. A model test estimating lateral and vertical acceleration was conducted using the strip theory method for automobiles based on their position on the car during side-wave conditions [10]

II. METHODOLOGY

This study focuses on a Ro-Ro ferry operating on the Bira-Pamatata shipping route. To evaluate the impact of various wave parameters on the ship's motion response, simulations are performed with changes in the wave heading angle, height, and wave length.

A. Numerical Simulations

The ferry, which operates on a relatively short route, is modeled in 3D using the Maxsurf modeler, and analyzed employing the Maxsurf motion method [21-24]. Figure 1 illustrates the hull shape and main dimensions of the Ro-Ro ferry, with a width (*B*) of 14.00 m, a height (*H*) of 7.11 m, and a length overall (*LOA*) of 56.00 m.

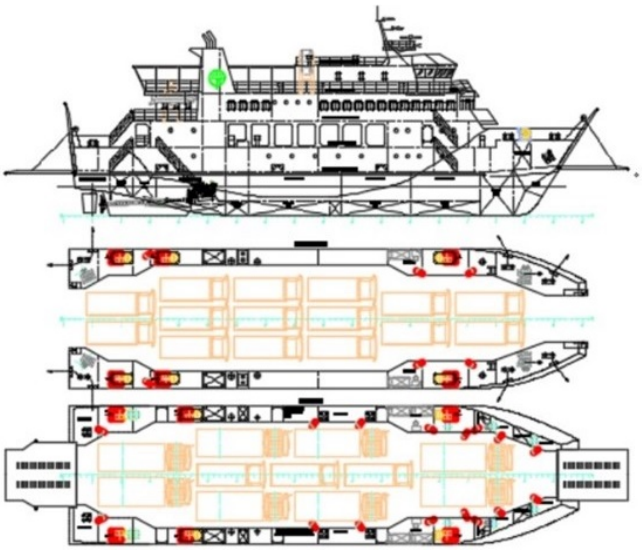

Fig. 1. General arragement of the Ro-Ro ferry.

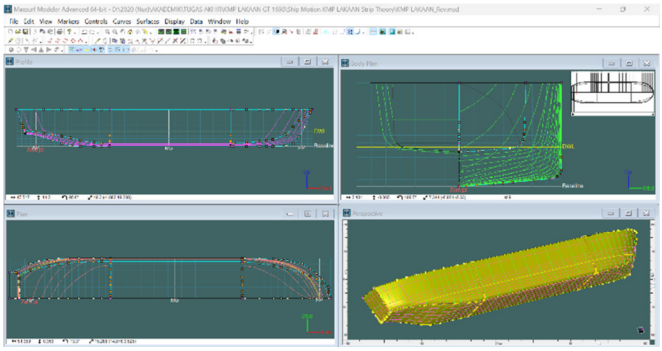

Fig. 2. 2D and 3D model of the line plan and hull .

The Computer Aided Design (CAD) model was developed using Maxsurf from the ground up, as a 3D-CAD formulation based on the ship's offset lines. The two-dimensional representations are projections of the 3D-CAD model, offering an additional perspective. The overall design of the ship is depicted in Figure 2.

In the ship motion analysis, "remote location" refers to the point where an object's center of gravity intersects with its load. The specified remote location is demonstrated in Figure 3.

(a)

	Name	Long. Pos.	Offset [m]	Height [m]	Long. Pos.	Offset from	Height fro	Mll slide fr	Mll tip fore	Mll tip side	Exposure
1	Avanza 1 (SB)	7.40	-3.19	4.32	-17.74	-3.19	0.32	0.70	0.17	0.25	120
2	Bus 2 (Center)	9.43	0.00	5.41	-15.71	0.00	1.41	0.70	0.17	0.25	120
3	Pick Up 3 (PS)	8.06	2.73	4.42	-17.08	2.73	0.42	0.70	0.17	0.25	120
4	Rush 4 (SB)	12.22	-2.71	4.32	-12.92	-2.71	0.32	0.70	0.17	0.25	120
5	Pick Up 5 (PS)	13.01	3.46	4.42	-12.13	3.46	0.42	0.70	0.17	0.25	120
6	BRV 6 (SB)	17.06	-3.22	4.31	-8.08	-3.22	0.31	0.70	0.17	0.25	120
7	Bus 7 (Center)	23.84	0.00	5.41	-1.30	0.00	1.41	0.70	0.17	0.25	120
8	Pick Up 8 (PS)	17.88	2.98	4.42	-7.26	2.98	0.42	0.70	0.17	0.25	120
9	Triton 9 (SB)	22.26	-2.68	4.35	-2.88	-2.68	0.35	0.70	0.17	0.25	120
10	Xenia 10 (PS)	22.89	2.78	4.31	-2.25	2.78	0.31	0.70	0.17	0.25	120
11	Fortuner 11 (SB)	28.12	-3.18	4.34	2.98	-3.18	0.34	0.70	0.17	0.25	120
12	Pick Up 12 (PS)	27.83	2.71	4.42	2.69	2.71	0.42	0.70	0.17	0.25	120
13	Hilux 13 (SB)	33.91	-3.51	4.36	8.77	-3.51	0.36	0.70	0.17	0.25	120
14	Bus 14 (Center)	38.27	0.00	5.41	13.13	0.00	1.41	0.70	0.17	0.25	120
15	Panther 15 (PS)	32.63	3.64	4.35	7.49	3.64	0.35	0.70	0.17	0.25	120
16	Voxy 16 (SB)	39.32	-3.06	4.30	14.18	-3.06	0.30	0.70	0.17	0.25	120
17	Innova 17 (PS)	37.65	2.71	4.34	12.51	2.71	0.34	0.70	0.17	0.25	120
18	Innova 18 (SB)	44.29	-3.19	4.34	19.15	-3.19	0.34	0.70	0.17	0.25	120
19	Innova 19 (PS)	43.48	2.91	4.34	18.34	2.91	0.34	0.70	0.17	0.25	120
20	Grammax 20 (SB)	49.04	-2.41	4.37	23.90	-2.41	0.37	0.70	0.17	0.25	120
21	Ayla 21 (Center)	48.80	0.00	4.22	23.66	0.00	0.22	0.70	0.17	0.25	120
22	Pick Up 22 (PS)	48.62	2.54	4.42	23.48	2.54	0.42	0.70	0.17	0.25	120

(b)

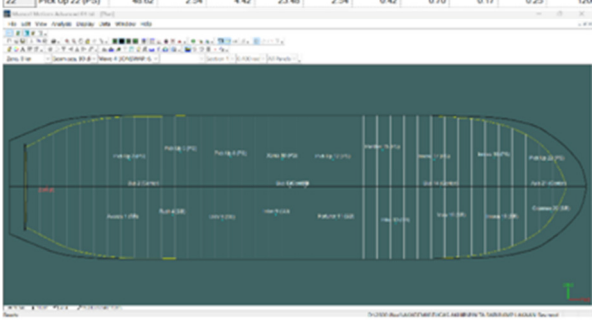

Fig. 3. (a) vehicle's main dimensions, (b) car deck plan.

After establishing the remote location and configuring the car deck layout, the setup is completed, with the ship being at zero knots. Additionally, the wave setup is prepared. The rolling behavior of the Ro-Ro ferry is influenced by the wave heading angle, which is set at 90 degrees (beam sea). JONSWAP wave profiles are employed, with significant wave heights and mean periods being selected based on the wave scatter diagram for the specified shipping area [25].

B. Waves

External forces, such as adverse environmental conditions, can generate large waves, water currents, and winds that pose risks to the ship, crew, and passengers while disrupting onboard comfort. To simplify the analysis and predict ship movements under these influences, several assumptions are made. Specifically, it is assumed that only sea waves are considered, with a wave heading of 90 degrees, as this is the angle at which roll motion exhibits the maximum response. Additionally, the waves are assumed to occur in deep-sea conditions to eliminate the influence of the seabed. The fundamental wave formulas used in the analysis are [26]:

$$L_w = \frac{2\pi}{g} \cdot V_w^2 = \frac{2\pi \cdot g}{\omega_w^2} = \frac{g \cdot T_w^2}{2\pi} \quad (1)$$

$$k = \frac{2\pi}{L_w} \quad (2)$$

$$T_w = \frac{1}{2} \cdot \left(\frac{2\pi \cdot L_w}{g}\right) \quad (3)$$

where L_w is the wavelength, V_w is the wave speed, T_w is the wave period, ω_w is the wave frequency, k is the wave number, and g is the gravitational acceleration.

The wave scatter on the Ro-Ro ferry route, Bira-Pamatata, is shown in Figure 4.

Significant wave height[m] \ relative peak period (smooth)[s]	0 - 1	1 - 2	2 - 3	3 - 4	4 - 5
0 - 0.5	0%	0.4%	10.4%	24.7%	17.4%
0.5 - 1	0%	0%	<0.1%	4.5%	11%
1 - 1.5	0%	0%	0%	0	0.4%
1.5 - 2	0%	0%	0%	0	<0.1%
2 - 2.5	0%	0%	0%	0	0%

Fig. 4. Wave scatter of the Ro-Ro ferry route.

C. Rolling Motion

The movement of a ship around its longitudinal axis is known as rolling motion. This motion alternates as the ship rolls from side to side, from the starboard to the port side. The ship's rolling motion can be analyzed using [27]:

$$a \cdot \frac{d^2\theta}{dt^2} + b \cdot \frac{d\theta}{dt} + c \cdot \theta = M_0 \cdot \cos(\omega_e t) \quad (4)$$

where $a\frac{d^2\theta}{dt^2}$ is the inertia moment, $b\frac{d\theta}{dt}$ is the damping moment, $c \cdot \theta$ is the restoring moment, and $M_0 \cdot \cos(\omega_e t)$ is the exciting moment.

The natural circular frequency of roll motion is:

$$\omega_{n\theta} = \sqrt{\frac{K_{44}}{I_{44}+a_{44}}} = \sqrt{\frac{\rho g \nabla GM_T}{I_{44}+a_{44}}} \quad (5)$$

where:

- K_{44} : roll motion stiffness (kN)
- I_{44} : moment of inertia of mass for roll motion (ton.m^2)

- a_{44}: additional mass moment of inertia for roll motion (ton.m^2)
- ρ: density of sea water (1.025 ton/m^3)
- g: gravinational acceleration (9.81 m/det^2)
- ∇: the volume displacement (m^3)
- GM_T: vertical position of the metacentric (m)

D. Newton Law

Newton's First Law of Motion states that an object will remain at rest or continue to move with constant velocity unless acted upon by an external force. The principle is often summarized as:

$$\Sigma F = 0 \quad (6)$$

Newton's Second Law establishes the relationship between a point object's kinematic quantities (acceleration, velocity, and displacement) and its dynamic quantities (mass and force). The second law states that the acceleration produced by the resultant force acting on an object is directly proportional to the resultant force, in the same direction, and inversely proportional to the mass of the object, and is expressed by:

$$\Sigma F = m \cdot a \quad (7)$$

The moment of force is defined as the rotational effect produced by a force acting at a distance from a pivot point. The moment is obtained by multiplying the applied force by the lever arm (the perpendicular distance from the axis of rotation to the line of action of the force). Mathematically, the moment of force can be expressed as:

$$\Sigma M = F \cdot L \quad (8)$$

where ΣM is the total moment, F is the applied force, and L is the lever arm.

The term moment of criteria refers to a quantity in rotational motion that is analogous to mass in translational motion. It measures an object's resistance to changes in its rotational motion around an axis. While mass resists changes in linear motion, the moment of inertia resists changes in rotation motion around a given axis [28]. To calculate the moment of inertia of a car with respect to its rotational axis, the moment of inertia formula is applied for a solid object rotating about an axis through its center of mass. This approach assumes the car behaves as a solid object. This provides insight into how resistant the vehicle is to changes in its rotational motion, which is essential for understanding its stability when subjected to rolling forces:

$$I = \frac{1}{2} mR^2 \quad (9)$$

III. RESULTS AND DISCUSSION

Table I presents the main dimensions of the Ro-Ro ferry studied. Data from the observations made on the Bira-Pamatata crossing route are presented in Table II and Figure 5. The analyzed ship, under a 90º wave heading angle and a ship speed of 0 knots, experienced the largest roll motion at a circular frequency of 0.912 rad/s. the largest pitch motion at a circular frequency of 0.823 rad/s, and the largest heave motion at a circular frequency of 1.214 rad/s. These results were obtained after inputting the required data for the ship's motion analysis. Figure 6 illustrates the motion response for each variation in wave height, presented in consecutive order.

TABLE I. DIMENSIONS OF THE RO-RO FERRY

	Values	Units
Overall Length (*LOA*)	56.09	m
Breadth (*B*)	14.00	m
Height (*H*)	7.11	m
Draft (*T*)	2.70	m
Gross Tonnage (*GT*)	1689	-

TABLE II. INTEREST OF VEHICLE DATA

Positioning from breadth	After Perpendicular	Midship	Fore Perpendicular
Starboard side	Avanza 1	Triton 9	Granmax 20
Center line	Bus 2	Bus 7	Ayla 21
Port side	Pick Up 3	Xenia 10	Pick Up 22

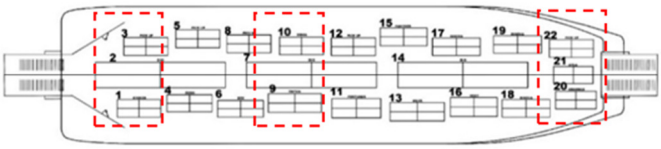

Fig. 5. Car deck plan of observations from Bira-Pamatata route.

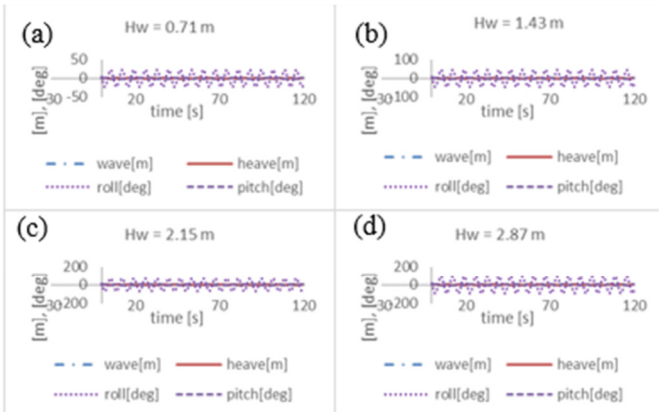

Fig. 6. Ship motion against wave height: (a) H_w = 0.71 m, (b) H_w = 1.43 m, (c) H_w = 2.15 m, (d) H_w = 2.87 m.

The results demonstrate that the wave height is directly proportional to the ship's motion in heave, roll, and pitch. The higher the wave is, the greater is the value of the produced ship motion.

Figure 7 outlines the lateral and vertical acceleration values of each vehicle, based on its dimensions, center of gravity, and position relative to the centerline and bus line. These accelerations are generated by the ship's motion under the influence of beam waves. The results reveal the significance impact of wave height on these accelerations. As the wave height increases, the vehicles experience higher lateral and vertical accelerations. However, there are differences in values across the vehicles. Notably, the lateral acceleration is consistently much higher than the vertical for all vehicles on

the car deck. Additionally, the positioning of the vehicles relative to the ship's width shows that the lateral acceleration values are nearly the same for vehicles located on the portside, starboard site, and centerline. In contrast, the vertical acceleration values on Bus 2 (CL) and Bus 7 (CL) are three times greater than those of the other vehicles.

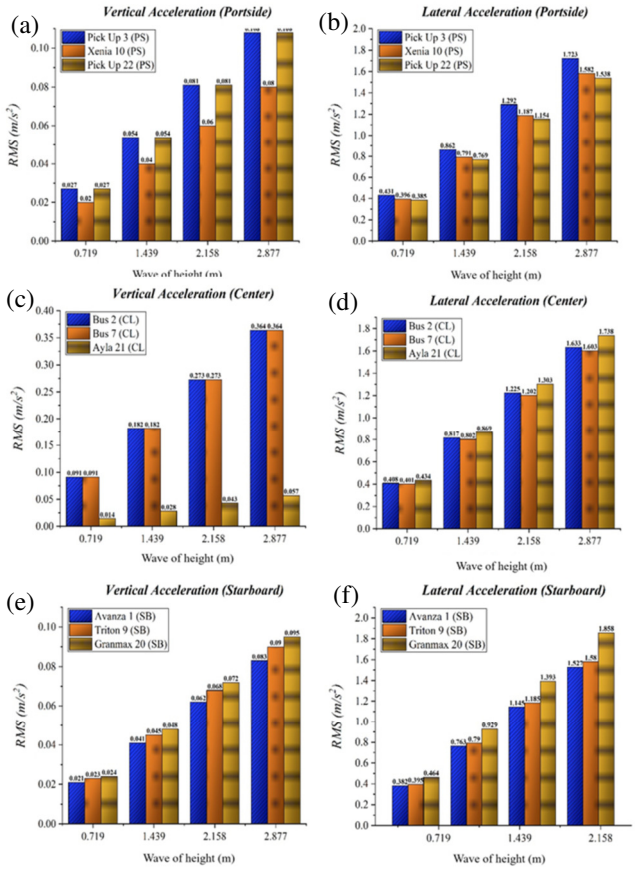

Fig. 7. Vertical and lateral acceleration of vehicle influence of/ the Beam Sea and wave heigth in varying wave heigth by using numerical simulation (a) vertical acceleration in port side, (b) lateral acceleration in port side, (c) vertical acceleration in centre, (d) lateral acceleration in centre, (e) vertical acceleration in starboard side, (f) lateral acceleration in starboard side.

A. The Maximum Angle of Heel Calculation

The force and moment balance formulae are applied to the lateral and vertical acceleration values of each vehicle, considering the maximum tilt angle resulting from the Ro-Ro ferry's heeling moment (Figure 8). This is performed to calculate the rolling moment of the vehicle. Additionally, the friction coefficient between the rubberized tires and the steel car deck is also factored into the data processing.

- Gravity vector along the x-axis:

$$W_x = m \cdot g \cdot sin\theta \quad (10)$$

- Gravity vector along the y-axis:

$$W_y = m \cdot g \cdot cos\theta \quad (11)$$

- Force equilibrium along the x-axis:

$$m \cdot g \cdot sin\theta - f_s = 0 \quad (12)$$

- Force equilibrium along the x-axis:

$$N - m \cdot g \cdot cos\theta = 0 \quad (13)$$

- Maximum tilt angle (θ_{max}):

$$m \cdot g \cdot sin\theta_{max} = \mu_s \cdot (m \cdot g \cdot cos\theta_{max})$$

$$tan\theta_{max} = \mu_s$$

$$\theta_{max} = tan^{-1}(\mu_s)$$

Substituting $\mu_s = 0.6$, we get:

$$\theta_{max} = 30.96°$$

The maximum tilt angle before the car begins to roll is approximately 30.96°. This indicates that the car will start to roll once the tilt angle reaches this threshold.

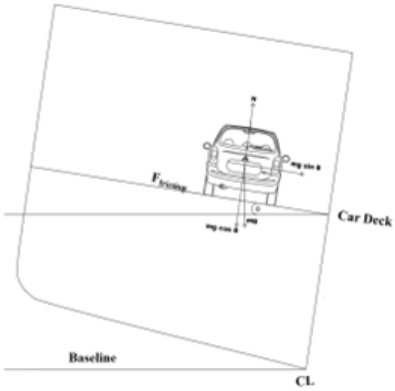

Fig. 8. Free-body diagram of the heeling maximum of vehicle.

Table III presents the roll moment values for each vehicle on the car deck of the Ro-Ro ferry, revealing key trends based on vehicle positioning and characteristics.

Bus 2 exhibits the largest roll moment, followed by Bus 7, with Ayla 21 showing the smallest roll moment. Notably, all three vehicles are positioned at the centerline of the car deck. However, the differences in their roll moments arise from variations in their size, mass, and positioning along the ship's length. Bus 2 is at After Peak, Bus 7 is at Midship, and Ayla 21 is at Fore Peak.

In addition to the longitudinal positioning, the mass and vertical center of gravity, relative to the car deck, significantly influence the roll moment value. For vehicles positioned on the portside and starboard side, similar tendencies are observed, aligning with findings from previous studies [4, 29]. Notably, even vehicles of the same type can exhibit different roll moments due to variations in the horizontal center of gravity, relative to the centerline. This is evident in the comparison of Pick Up 3 and Pick Up 22, where Pick Up 3 has a greater roll moment because its horizontal center of gravity is farther from the centerline than that of Pick-up 22.

TABLE III. SUMMARIZED DATA OF ROLLING MOMENT OF VEHICLES

Vehicle	$H_{vertical}$ (m)	Inertia or limits (N·m)	$F_{friction}$ (N)	$F_{resulant}$ (N)	M_{roll} (N·m)
Pick Up 3 (PS)	0.950	2496.25	9114	2676	2537
Xenia 10 (PS)	0.840	1644.99	6350	1711	1436
Pick Up 22 (PS)	0.950	2496.25	9114	2458	2329
Bus 2 (CL)	1.940	11120.80	26672	7589	14370
Bus 7 (CL)	1.940	11120.80	26672	7456	14106
Ayla 21 (CL)	0.750	1190.81	5154	1522	1141
Avanza 1 (SB)	0.850	1866.44	6145	1598	1356
Triton 9 (SB)	0.880	2890.40	9161	2466	2167
Granmax 20 (SB)	0.900	3150.03	11466	3628	3261

IV. CONCLUSIONS

This study identifies the potential for vehicle shifting on Ro-Ro ferries using numerical simulations to calculate vehicle shear and overturning moments. The results indicate that Bus 2 (CL), positioned at the rear of the ship, has the highest potential to overturn, with a rolling moment of 14,370 N·m, which exceeds its moment of inertia limit of 11,120.80 N·m. In contrast, Ayla 21 (CL), located at the front, has the lowest overturning potential, with a rolling moment of 1,141 N·m, well below its moment of inertia limit.

The magnitude of the rolling moment is significantly influenced by three factors:

- The mass of the vehicle.
- The horizontal center of gravity of the vehicle, relative to the centerline.
- The vertical center of gravity, relative to the car deck.

The rolling moment increases with greater distances between the vertical center of gravity and the car deck, as well as the horizontal center of gravity and the centerline. Conversely, a reduction in these distances results in a lower rolling moment.

ACKNOWLEDGMENT

This research was funded by a grant from the Ministry of Education, Culture, Research, and Technology of Indonesia (037/E5/PG.02.00.PL./2024 and 6465/IT10.II/PPM.04/2024).

REFERENCES

[1] D. Faturachman and S. Mustafa, "Performance of Safety Sea Transportation," *Procedia - Social and Behavioral Sciences*, vol. 57, pp. 368–372, Oct. 2012, https://doi.org/10.1016/j.sbspro.2012.09.1199.

[2] J. Chen, J. Yang, K. Shen, Z. Chang, and Z. Zheng, "Probability Density Analysis of Nonlinear Random Ship Rolling," *Journal of Ocean University of China*, vol. 22, no. 5, pp. 1227–1242, Oct. 2023, https://doi.org/10.1007/s11802-023-5323-0.

[3] Z. Jiang, Y. Ma, and W. Li, "A Data-Driven Method for Ship Motion Forecast," *Journal of Marine Science and Engineering*, vol. 12, no. 2, Feb. 2024, Art. no. 291, https://doi.org/10.3390/jmse12020291.

[4] D. Paroka, A. H. Muhammad, and S. Rahman, "Hydrodynamics factors correspond to the weather criterion applied to an Indonesian Ro-Ro Ferry with different weight distributions," *International Journal of Technology*, vol. 12, no. 1, pp. 126–138, Jan. 2021, https://doi.org/10.14716/ijtech.v12i1.4246.

[5] K. E. Marlantes and K. J. Maki, "A hybrid data-driven model of ship roll," *Ocean Engineering*, vol. 303, Jul. 2024, Art. no. 117821, https://doi.org/10.1016/j.oceaneng.2024.117821.

[6] Z. Jovanoski and G. Robinson, "Ship Stability and Parametric Rolling," *Australasian Journal of Engineering Education*, vol. 15, no. 2, pp. 43–50, Jan. 2009, https://doi.org/10.1080/22054952.2009.11464028.

[7] X. Wang, Z. Liu, S. Loughney, Z. Yang, Y. Wang, and J. Wang, "An experimental analysis of evacuees' walking speeds under different rolling conditions of a ship," *Ocean Engineering*, vol. 233, Aug. 2021, Art. no. 108997, https://doi.org/10.1016/j.oceaneng.2021.108997.

[8] S. Fang, Z. Liu, X. Wang, Y. Cao, and Z. Yang, "Dynamic analysis of emergency evacuation in a rolling passenger ship using a two-layer social force model," *Expert Systems with Applications*, vol. 247, Aug. 2024, Art. no. 123310, https://doi.org/10.1016/j.eswa.2024.123310.

[9] B. Göksu, "Stability of a Ro-Ro Ship: An Assessment of the Impact of Electric Vehicle Transportation," *Journal of Marine and Engineering Technology*, vol. 4, no. 1, pp. 11–21, Jun. 2024, https://doi.org/10.58771/joinmet.1397687.

[10] Alamsyah, W. Setiawan, D. Paroka, N. Nurbaya, H. S. Sitanggang, and M. R. F. Jaya, "Characteristics of Lateral Acceleration and Vertical Acceleration of the Position of the Vehicle on the Ferry Ro-Ro Car Deck," *International Journal of Marine Engineering Innovation and Research*, vol. 8, no. 3, pp. 530–534, Sep. 2023, https://doi.org/10.12962/j25481479.v8i3.18792.

[11] P. Crossland and K. Rich, "A method for deriving MII criteria," in *Conference on Human Factors in Ship Design and Operation, London, UK*, 2000.

[12] A. E. Baitis *et al.*, "1992 motion induced interruptions (MII) and motion induced fatigue (MIF) experiments at the Naval Biodynamics Laboratory," *Techn. Rep. No. CRDKNSWC-HD-1423-01, Naval Surface Warfare Center*, 1991.

[13] R. I. Kemenhub, *Peraturan Menteri Perhubungan Republik Indonesia Nomor PM 115 TAHUN 2016 Tentang Tata Cara Pengangkutan Kendaraan Di Atas Kapal*. 2016.

[14] R. I. Kemenhub, *Peraturan Menteri Perhubungan Republlk Indonesia Nomor PM 30 TAHUN 2016 Tentang Kewajiban Pengikatan Kendaraan Pada Kapal Angkutan Penyeberangan*. 2016.

[15] A. Alamsyah, A. Hidayatullah, S. Suardi, W. Setiawan, H. Habibi, and S. D. Nurcholik, "Motion Response on The Water Ambulance Ship," *International Journal of Marine Engineering Innovation and Research*, vol. 8, no. 1, Feb. 2023, https://doi.org/10.12962/j25481479.v8i1.15481.

[16] D. Paroka, S. Asri, Rosmani, and Hamzah, "Alternative Assesement of Weather Criterion for Ships with Large Breadth and Draught Ratios by a Model Expirement: a Case Study on an Indonesian Ro-Ro Ferry," *International Journal of Maritime Engineering*, vol. 162, no. A1, 2020, https://doi.org/10.5750/ijme.v162iA1.1121.

[17] D. Paroka, "Yaw Motion Stability of an Indonesian Ro-Ro Ferry in Adverse Weather Conditions," *International Journal of Technology*, vol. 11, no. 4, pp. 862–872, 2020, https://doi.org/10.14716/ijtech.v11i4.2852.

[18] A. H. Muhammad, D. Paroka, S. Rahman, M. R. Firmansyah, and T. P. Putra, "Characteristics of Turning Circle and Zig-Zag Manoeuvres of An Indonesian Ferry Ship In Shallow Water," *IOP Conference Series: Materials Science and Engineering*, vol. 1052, no. 1, Jan. 2021, Art. no. 012036, https://doi.org/10.1088/1757-899X/1052/1/012036.

[19] D. Paroka, A. H. Muhammad, and S. Rahman, "Safety of an Indonesian ro-ro ferry with different weight distribution on vehicle deck," *AIP Conference Proceedings*, vol. 2543, no. 1, Nov. 2022, Art. no. 080009, https://doi.org/10.1063/5.0094745.

[20] D. Paroka, A. H. Muhammad, S. Rahman, and F. M. Assidiq, "Vulnerability of Ship with a Large Breadth to Draught Ratio Against Excessive Acceleration Criteria," *IOP Conference Series: Earth and Environmental Science*, vol. 1166, no. 1, Feb. 2023, Art. no. 012008, https://doi.org/10.1088/1755-1315/1166/1/012008.

[21] L. Xing-yu, H. Yan-ping, and C. Chao, "Analysis of the Seakeeping Performance of Icebreaker Based on Maxsurf," in *The 30th International Ocean and Polar Engineering Conference*, Virtual, Oct. 2020, pp. 664-672.

[22] G. Younis, R. R. Abdelghany, M. M. Mostafa, and R. El-Barbary, "Sensitivity Analyses of Intact and Damage Stability Properties to Passenger Ship's Dimensions and Proportions," *Port-Said Engineering Research Journal*, vol. 23, no. 1, pp. 65–73, Mar. 2019, https://doi.org/10.21608/pserj.2019.32861.

[23] G. Guan, L. Wang, J. Geng, and Q. Yang, "Automatic optimal design of self-righting deck of USV based on combined optimization strategy," *Ocean Engineering*, vol. 217, Dec. 2020, Art. no. 107824, https://doi.org/10.1016/j.oceaneng.2020.107824.

[24] S. Anggara, R. D. Maskar, M. R. F. Hariadi, L. M. Ichsan, M. Zaky, and A. Kurniawan, "The Application of 2nd Generation Intact Stability Criteria to Ship Operating in Indonesia Waterway: Pureloss Stability," *IOP Conference Series: Materials Science and Engineering*, vol. 1052, no. 1, Jan. 2021, Art. no. 012050, https://doi.org/10.1088/1757-899X/1052/1/012050.

[25] K. Hasselmann *et al.*, "Measurements of wind-wave growth and swell decay during the joint North Sea wave project (JONSWAP).," *Ergänzungsheft zur Deutschen Hydrographischen Zeitschrift, Reihe A*, vol. Nr. 12, 1973.

[26] R. Bhattacharyya, *Dynamics of Marine Vehicles*, New York, USA: John Wiley & Sons, 1978.

[27] E. B. Djatmiko, *Perilaku dan Operabilitas Bangunan Laut di Atas Gelombang Acak*, Surabaya: ITS Press, 2012.

[28] Y. Chen, Y. Zeng, H. Li, J. Zhang, and L. Zhang, "Research on the Measurement Technology of Rotational Inertia of Rigid Body Based on the Principles of Monocular Vision and Torsion Pendulum," *Sensors*, vol. 23, no. 10, Jan. 2023, Art. no. 4787, https://doi.org/10.3390/s23104787.

[29] P. Crossland and K. Rich, "Validating a model of the effects of ship motion on postural stability," in *International Conference of Environmental Ergonomics*, 1998, vol. 77, pp. 385–388.